Experimental investigation of the processes determining x-ray emission intensities from charge-exchange collisions

J. B. Greenwood,[1,*] I. D. Williams,[1,†] S. J. Smith,[2,‡] and A. Chutjian[2,§]
[1]*Physics Department, The Queen's University of Belfast, Belfast BT7 1NN, United Kingdom*
[2]*Jet Propulsion Laboratory, California Institute of Technology, Pasadena, California 91109*
(Received 26 December 2000; published 8 May 2001)

Absolute cross sections have been measured for single and double charge exchange and x-ray line emission for highly charged ions of C, N, O, and Ne colliding with He, H_2, CO_2, and H_2O at collisions energies of $7q$ keV. Present results of charge exchange in He and H_2 compare favorably with previous results. For CO_2 and H_2O, where prior work is scarce, the classical overbarrier model is found to overestimate results by up to a factor of 3. An analysis of the relative intensities of the observed Lyman x-ray transitions indicates that capture into l states is not statistical, as collision velocities are insufficient to populate the highest angular-momentum states. The importance of autoionization following multiple capture is highlighted, and enhanced radiative stabilization following double capture is observed and compared to other studies. Present results are also discussed in terms of mechanisms likely to generate x-ray emission in comets.

DOI: 10.1103/PhysRevA.63.062707 PACS number(s): 34.50.Gb, 82.30.Fi, 96.60.Vg

I. INTRODUCTION

Electron capture by highly charged ions (HCI's) plays an important role in understanding the interaction of high-temperature plasmas with cold gases. The minor constituents of the solar wind (C, N, O, Ne, Mg, Si, Fe), as well as impurities in magnetically confined fusion machines exist in highly charged states. These ions interact with planetary, cometary, and interstellar gases, or with cold gas injected into the divertor region of tokamaks. In these plasmas, as the cross sections are large (10^{-15}–$10^{-14}\,\mathrm{cm}^2$) compared to other atomic processes, capture is usually the dominant process. Excited states are populated in the product ion, and if the ion charge q is large the radiative decays have short wavelengths. These provide an important source of x rays in astronomical objects. In particular, charge exchange is to date the most convincing explanation for the recent and unexpected discovery of x-ray emission from comets [1–10]. It could also provide an important contribution to the soft-x-ray background [11] and to the Jovian x-ray emissions [12].

The electron-capture reaction proceeds as

$$A^{q+} + X \rightarrow (A^{(q-i)+})^* + X^{i+} \rightarrow A^{(q-j)+} + X^{k+} + (k-j)e^- + N(h\nu), \qquad (1)$$

where $N(h\nu)$ is the number of emitted x-ray photons. The intermediate ion $(A^{(q-i)+})^*$ is formed in an excited state through the capture of i electrons from a target X. The final ion $A^{(q-j)+}$ has j electrons more than the incident ion. In this paper $j=1$ is referred to as single exchange, $j=2$ as double exchange, with $i=2$ as double capture, etc.

*Email address: j.greenwood@qub.ac.uk
†Email address: i.williams@qub.ac.uk
‡Email address: steven.j.smith@jpl.nasa.gov
§Email address: ara.chutjian@jpl.nasa.gov

Although measurements of charge exchange for singly charged ions have been carried out for many years [13], it is only in the last 25 years that development of powerful ion sources has enabled measurements using HCI's. Moreover, the work has mostly focused on collisions with H, H_2, and He targets [14,15]. These are the simplest systems to study theoretically and have applications to fusion and astrophysical plasmas. However, there has been little experimental work on collisions with more complex molecular targets. A full quantal formulation requires the consideration of a large number of curve crossings associated with the quasimolecule formed in the collisions with molecular targets. Such theoretical studies have so far been limited to H_2 [16–18].

The classical overbarrier model (OBM) was developed by Ryufuku *et al.* [19] for obtaining estimates of cross sections. It was later extended by Niehaus [20] to include multiple capture and the concept of a reaction window. As the calculations are analytical, and depend only on the charge state q and the ionization potential of the target, the analytical model is convenient for plasma computer models. The simple OBM predicts the n level into which capture predominately occurs. It does not take into account the collision velocity or the l state of the captured electron.

Burgdörfer *et al.* [21] modified the OBM by including a centrifugal term to take into account the angular momentum of the captured electron. The distribution of l states within a single n shell has been investigated by a number of authors [22–25]. These studies show that l selectivity is difficult to predict and, unlike the total cross sections, can vary strongly with collision energy. Comparison of this model with experiment [21] shows that the average value $\langle l \rangle$ for the angular momentum of the captured state can be predicted. At low collision velocities the captured electron does not possess enough angular momentum to populate high l states. However, as the velocity reaches one-half the orbital velocity of the electron, the states are expected to be populated statistically. As noted by Janev and Winter [24] this agrees with predictions of quantum-mechanical models in the case of strong rotational coupling of Stark states, which occurs in

systems where there is near degeneracy of l levels (i.e., for bare projectiles and highly charged ions). At low collision energies it is predicted that the distribution will peak at $l=1$ [26].

For single capture by bare projectiles it is difficult to measure the l-state distributions due to their degenerate nature. Hoekstra *et al.* [27] were able to do so for the $He^{2+}+H$ system by observing visible and UV photon emission at different points downstream from the collision. For higher charge states the lifetimes become too short to use this method. Vernhet *et al.* [23] used x-ray spectroscopy to observe Lyman transitions from capture by bare and H-like projectiles. They used the ratios of these transitions to determine the average angular momentum of the initial state.

The effects of autoionizing double-capture contributions to the single-exchange cross section have received considerable attention [28–35]. Of particular interest are mechanisms that govern the ratio between stabilization and autoionization of doubly excited states formed in double capture. Although the two electrons in these states are often captured into similar n levels ($n_1 \approx n_2$), formation of asymmetric states ($n_1 > n_2$) can occur through mixing with the symmetrical configurations (autotransfer to Rydberg states), or directly through a transfer excitation process. By studying a wide range of fully stripped projectiles and targets Martin *et al.* [33] showed how the population of asymmetric states enhances the stabilization ratio.

Presented herein is an experimental arrangement used to obtain accurate absolute cross sections for single and multiple exchanges by HCI's in various gases [36,37]. The apparatus includes a viewing port in the target-gas cell for observations of x rays produced in the collisions. Use is made of a pure Ge solid-state x-ray detector. The present absolute results are compared to data obtained from previous experiments, and are used to discuss the effectiveness of the OBM at predicting cross sections. The observed x-ray spectra correspond to the Lyman (Ly) series emission lines generated from excited states of He and H-like oxygen and neon ions. Line emission cross sections are reported. The relative intensities of these lines are used to discuss the l-state distribution of the initial capture states. The contribution of double capture to both single and double exchange is also discussed.

II. EXPERIMENTAL METHOD

The ions of interest are produced at the JPL HCI facility [38]. The ions are extracted from an electron cyclotron resonance (ECR) ion source at a potential of +7 kV. They are focused and deflected into a 90° double-focussing bending magnet that selects the desired mass-to-charge ratio. As fully stripped ions of C, N, O, and Ne have the same mass-to-charge ratio as H_2^+, isotopically enhanced gases (^{13}CO, $^{15}N_2$, $^{18}O_2$, and ^{22}Ne) were used to produce the beams.

The selected ion beam is deflected and focused into the charge-exchange beam line, shown schematically in Fig. 1. The base vacuum here is less than 10^{-8} mbar. A high degree of collimation is achieved using three small apertures before the beam enters the gas cell. The cell (60.8 mm in length) has entrance and exit apertures of 0.75 and 2.5 mm diameter, respectively. A gas line is connected to the cell by a large-diameter flexible bellows. The pressure of this line is monitored just outside the chamber by a temperature-stabilized capacitance manometer capable of measurements to an accuracy of 5×10^{-6} mbar. As the conductance between the gas cell and the capacitance manometer is large, there is only a small pressure differential between the two. Using known dimensions of the connecting tubes and the apertures, this difference is calculated to produce a 15% pressure drop from the manometer to the cell. This calculation may introduce a 2% systematic error to the absolute pressure measurement. Typical pressures inside the cell during a run are $(5-10)\times10^{-5}$ mbar.

Consideration is also made of the temperature difference between the collision cell and capacitance manometer when determining the pressure of gas in the cell. The cell is maintained at room temperature ($T_2=295$ K) while the manometer is temperature stabilized at $T_1=318$ K. For a gas at two temperatures separated by an aperture, Knudsen [39] determined the pressure drop to be $(T_2/T_1)^{1/2}=0.96$ across the interface. However, Blaauw *et al.* [40] found that this formula does not work well for tubes, the ratios being closer to unity. A value of 0.99 ± 0.01 obtained by Bromberg [41] is used for the similar temperatures and tube diameters herein.

The charge-exchange cell apertures are small enough to produce a pressure differential between the gas cell and the chamber exceeding 100. Additional differential pumping between the chamber, the ion beam line, and the ECR source ensures that source conditions are unaffected by the introduction of gas into the cell. Gas is admitted into the cell by an UHV leak valve connected to research-grade gas cylinders. Before measurements, the gas line is evacuated to pressures less than 10^{-2} mbar and then pressurized to several atmospheres. For measurements with H_2O as the target, a vial of distilled water was frozen, pumped, and thawed multiple times to remove any dissolved gases.

To determine the effective target length of the gas, one notes that if the pressure inside the cell is assumed to be constant, effusion of gas from the cell apertures introduces an additional target length often assumed to be equal to the sum of the radii of the apertures. Alternatively, measurements by Blaauw *et al.* [40] and Mathur *et al.* [42] indicate the effective length is closer to the cell length itself, a conclusion used here. As the length of the present cell is large compared to the diameter of the apertures, the systematic error in determining the target gas length is small (<2%).

Beam currents are measured in a Faraday cup having a large diameter/length ratio of 15. The current is also monitored on the surrounding shield to ensure that all of the ions enter the cup and that no secondary electrons escape. The proximity of the Faraday cup to the collision cell ensures a large collection angle for the scattered ions (1.5° from the entrance aperture, 2° from the exit).

An ion undergoing charge exchange in the collision cell has a kinetic energy close to that of the incident ion. The potential required to reflect an ion that has undergone exchange of j electrons is

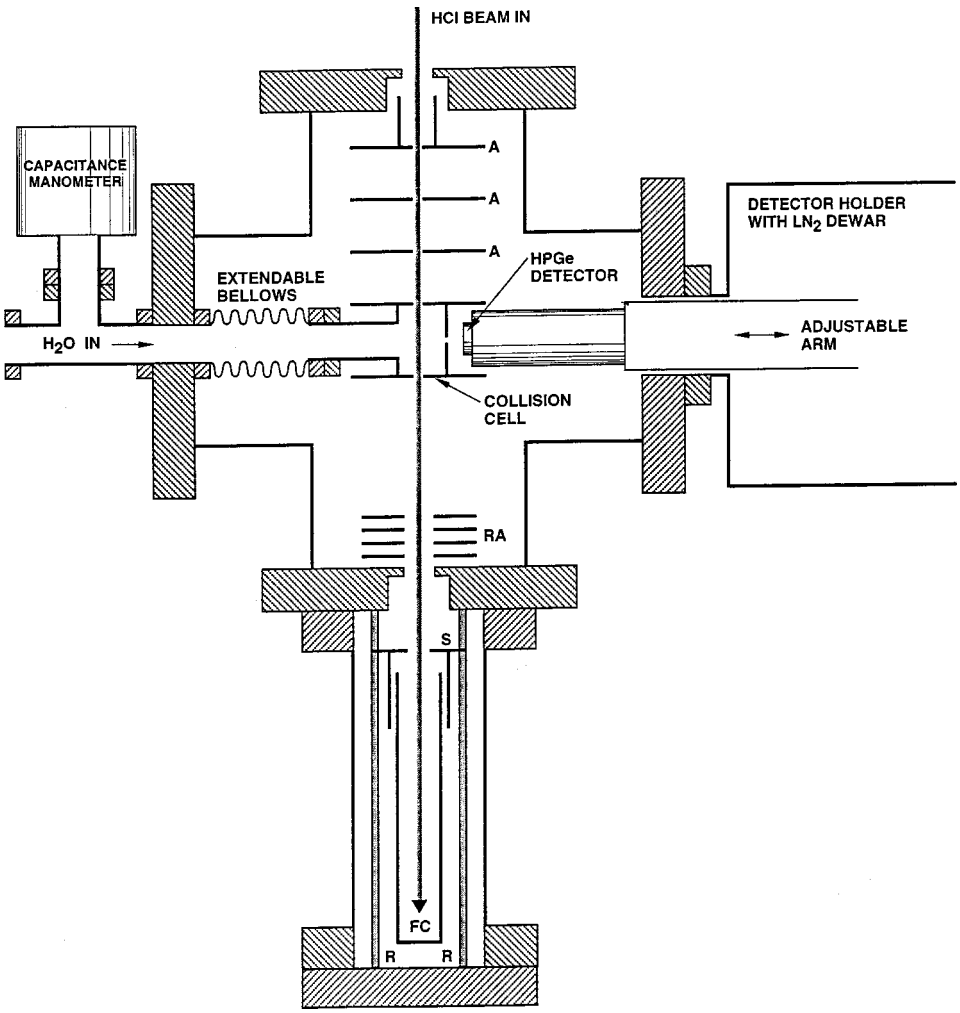

FIG. 1. Details of the charge-exchange beamline. The definitions are A, input HCI beam-defining apertures; RA, retarding-field apertures; S, secondary-electron shield; FC, Faraday cup; R, support rods; LN_2, liquid nitrogen.

$$V_R = \frac{qV_0}{(q-j)}, \tag{2}$$

where V_0 is the source voltage. Thus, it is possible to reflect the primary ion beam while charge-exchanged ions are transmitted. By raising this reflecting potential, ion currents from single and multiple charge exchanges are measured. This electric field is produced by a series of four apertures, the center two are held at the required reflecting potential, the end two at ground potential. The apertures have a large diameter and are widely spaced to give field lines that are almost parallel near the beam axis. They are also placed close to the Faraday cup to ensure that all transmitted ions are collected.

The pressure of gas in the cell is held low so that only about 1% of the ion beam charge exchanges, ensuring single-collision conditions. The cross section for the charge exchange is determined from the relationship

$$\sigma_{q,q-j} = \frac{kT}{PL}\frac{qI_{q-j}}{(q-j)I_q}, \tag{3}$$

where L is the collision length, T the gas temperature, I_q and I_{q-j} the measured primary and secondary currents, respectively, and P the gas pressure. The primary I_q and secondary currents I_{q-j} are measured in the same Faraday cup using the same electrometer and scale. Hence any systematic error in the absolute current measurement is eliminated in the above formula. This is an advantage over the use of channel-type multipliers, for which a linear response to ion current must be assumed. Electrometer and capacitance manometer zero offset and drift are taken into account when making measurements.

Errors in the measurements mainly arise from the pressure measurement and instability of the ion beam. As I_{q-j} and I_q cannot be measured simultaneously, a drift in ion beam current is unwelcome. In practice I_{q-j} and I_q are measured alternately multiple times, and the measurements of $\sigma_{q,q-j}$ are averaged. The standard deviation of these results is used to determine the random error due to the variability of the ion beam.

A 2-mm aperture in the cell wall allows x-rays to escape. A high-purity Ge solid state EG&G IGLET-*X* detector [43] with a high detection efficiency and moderate resolution is located at right angles to the beam axis. A 7.5-μm-thick Be window isolating the detector from the vacuum chamber introduces a transmission factor dependent on the energy of the x rays. The detector can be translated inside a flexible bellows to place it close to the aperture in the cell. At full extension, a 10 mm length of the ion beam can be ob-

TABLE I. Absolute charge-exchange cross sections for the neutral targets H_2O, CO_2, H_2, and He for the highly charged ions indicated. Cross sections are in units of $10^{-15}\,cm^2$, and errors are given at the 1σ confidence level.

		$^{13}C^{3+}$	$^{13}C^{6+}$	$^{15}N^{4+}$	$^{15}N^{7+}$	$^{16}O^{5+}$	$^{18}O^{7+}$	$^{18}O^{8+}$	$^{27}Ne^{9+}$
H_2O	$\sigma_{q,q-1}$	1.5±0.1	6.0±1.4	2.9±0.2	9.5±1.4	4.3±0.5	5.3±0.8	6.3±0.7	8.0±2.0
	$\sigma_{q,q-2}$	0.8±0.1	0.8±0.7	0.7±0.1	2.0±0.4	0.4±0.1	0.8±0.1	1.5±0.5	1.2±1.2
	$\sigma_{q,q-3}$				<0.3	0.3±0.2	<0.3	<0.3	
CO_2	$\sigma_{q,q-1}$	1.1±0.1	5.1±1.0	4.1±0.6	7.1±0.6	4.1±0.5	6.8±1.4	6.3±0.7	7.2±1.8
	$\sigma_{q,q-2}$	1.2±0.1	1.3±0.6	1.1±0.1	2.6±0.4	0.6±0.1	1.1±0.2	2.1±0.5	2.0±1.7
	$\sigma_{q,q-3}$				<0.3	0.6±0.1	0.3±0.1	<0.5	
H_2	$\sigma_{q,q-1}$	0.69±0.02	4.4±0.8	3.5±0.5	4.8±0.9	2.6±0.14	4.5±0.4	5.3±0.5	4.1±2.5
	$\sigma_{q,q-2}$	0.36±0.04	<0.7	0.09±0.04	<0.6	<0.06	<0.2	0.7±0.2	<2.6
He	$\sigma_{q,q-1}$	1.07±0.3	1.5±0.2	0.31±0.01	2.0±0.2	1.7±0.1	1.8±0.1	2.8±0.2	2.4±0.3
	$\sigma_{q,q-2}$	<0.06	0.2±0.1	0.24±0.01	<0.2	0.12±0.02	0.07±0.03	0.2±0.1	<0.6

served with a solid angle collection efficiency of about 0.1%. The emission angles with respect to the beam axis accepted by the active surface of the detector are in the range $90 \pm 15°$.

III. RESULTS

A. Total cross sections

Total cross sections for single, double, and in some cases, triple charge exchange of Li-like, H-like, and bare ions of C, N, O, and Ne in collision with He, H_2, H_2O, and CO_2 at an energy of $7q$ keV are listed in Table I. Total errors are presented at one standard deviation confidence level. The ion beams are expected to be in their ground-state configuration due to the absence of metastable levels. For the H-like ions used (O^{7+} and Ne^{9+}) it is noted that the intensity of the fully stripped ions (O^{8+}, Ne^{10+}) under the same source conditions is more than an order of magnitude smaller. This suggests that the electron temperature in the ion source is not high enough to significantly populate the high-lying $2s$ metastable levels. This hypothesis was checked by showing that there was no change in measurements for different microwave power inputs to the source.

In Table II we list previous results [14,44–49] and compare with present data. There have been a number of investigations for collisions with H_2 and He, but limited studies for CO_2 and H_2O. In most cases the agreement is within uncertainties, confirming the accuracy of our methods. The determination of target thickness was demonstrated in a previous paper [36], where a measurement of single exchange of

TABLE II. Comparisons of present absolute charge-exchange cross sections ($10^{-15}\,cm^2$) with results of previous studies (at energies given in parentheses). Errors are given at the 1σ confidence level.

Collision system	Process	Energy (keV/amu)	Cross section	Previous work
$^{13}C^{3+}+CO_2$	$\sigma_{q,q-1}$	1.62 (2.08)	1.1±0.1	1.0±0.1 [44]
	$\sigma_{q,q-2}$		1.2±0.1	1.0±0.1 [44]
$^{13}C^{3+}+H_2$	$\sigma_{q,q-1}$	1.62 (1.58, 1.4)	0.69±0.02	0.64±0.5 [44], 0.58±0.09 [45]
	$\sigma_{q,q-2}$		0.36±0.04	0.36±0.03 [44]
$^{13}C^{3+}+He$	$\sigma_{q,q-1}$	1.62 (1.7)	1.07±0.03	1.6±0.5 [14]
$^{13}C^{6+}+H_2$	$\sigma_{q,q-1}$	3.23 (2.0)	4.4±0.8	4.4±0.7 [14]
$^{13}C^{6+}+He$	$\sigma_{q,q-1}$	3.23 (2.0)	1.5±0.2	0.9±0.4 [14]
$^{15}N^{4+}+H_2$	$\sigma_{q,q-1}$	1.87 (1.8)	3.5±0.5	3.2±0.5 [45]
$^{15}N^{4+}+He$	$\sigma_{q,q-1}$	1.87 (1.87)	0.31±0.01	0.27±0.07 [46]
	$\sigma_{q,q-2}$		0.24±0.01	0.22±0.07 [46]
$^{15}N^{7+}+He$	$\sigma_{q,q-1}$	3.27 (3.0, 3.1)	2.0±0.2	1.9±0.2 [47], 1.8 [48]
$^{16}O^{5+}+H_2$	$\sigma_{q,q-1}$	2.19 (1.87, 1.63)	2.6±0.14	2.2±0.3 [45], 2.0±0.03 [49]
$^{16}O^{5+}+He$	$\sigma_{q,q-1}$	2.19 (2.19)	1.7±0.1	1.7±0.4 [46]
	$\sigma_{q,q-2}$		0.12±0.02	0.10±0.03 [46]
$^{18}O^{7+}+H_2$	$\sigma_{q,q-1}$	2.72 (2.0)	4.5±0.4	3.3±0.5 [14]
$^{18}O^{7+}+He$	$\sigma_{q,q-1}$	2.72 (2.0)	1.8±0.1	1.6±0.5 [14]
$^{18}O^{8+}+H_2$	$\sigma_{q,q-1}$	3.11 (4.0)	5.3±0.5	4.9±0.7 [14]
$^{18}O^{8+}+He$	$\sigma_{q,q-1}$	3.11 (4.0)	2.8±0.2	3.0±0.9 [14]

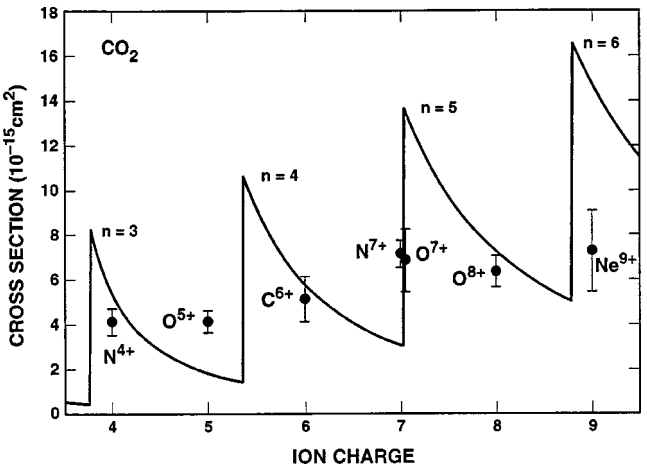

FIG. 2. Single charge-exchange cross sections in CO_2 compared to predictions of the classical overbarrier model (solid line).

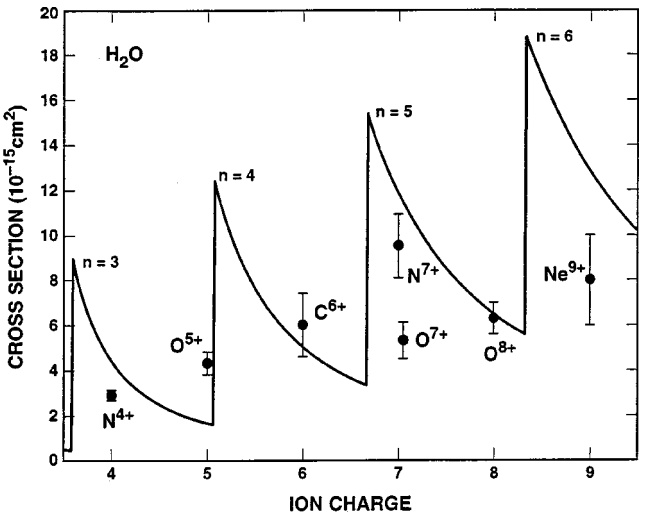

FIG. 3. Single charge-exchange cross sections in H_2O compared to predictions of the classical overbarrier model (solid line).

H^+ in H_2O with a total error of 5%, showed agreement with an equally accurate result [50]. As product ions suffer a small deflection due to Coulomb repulsion in the exit channel, additional checks were made to ensure all these ions were collected in the Faraday cup. Measurements were repeated using different-diameter apertures to vary the angular acceptance. No significant change in the measured cross sections was observed.

Due to the lack of data on collisions with H_2O and CO_2 the single-exchange cross sections were compared to those estimated by the OBM. Here, the principal quantum number n of the captured electron is predicted to be the largest integer satisfying the inequality [19],

$$n \leqslant q\left[2I_P\left(1+\frac{q-1}{2\sqrt{q}+1}\right)\right]^{-1/2}, \tag{4}$$

where I_P is the ionization potential of the target. The crossing distance R_C for hydrogenic systems is

$$R_C = \frac{q-1}{\frac{q^2}{2n^2}-I_P}. \tag{5}$$

The cross section, given by πR_C^2, assumes that for many-electron targets there is on average a probability of unity for the electron to remain bound to the ion as the two centers separate. Predictions of this model for a projectile of charge q interacting with CO_2 and H_2O are shown in Figs. 2 and 3, and compared to the present results for single capture. One sees that discontinuities in the OBM—due to capture occurring into different n shells—is poorly reproduced by the present data. This is an indication that the capture state n is not unique, and that a range of states is populated. This is also evident from previous state-selective capture measurements [51]. Present results for the systems O^{7+}, $N^{7+}+H_2O$ also show that the cross sections are not solely dependent on charge state q.

For some lower charge states (e.g., C^{3+}, N^{4+}) it is seen that the double-exchange cross section is comparable to the single-exchange value. This can be explained by the concept of the ''reaction window'' referred to in both the extended overbarrier model [20] and the Landau-Zener model [52]. The absence of available single-capture channels within this window increases the importance of double-capture channels. For other ions, the double exchange in H_2O and CO_2 is still a large proportion of the single-exchange cross sections. This is not the case for He and H_2. This suggests that autoionization following multiple capture is important. As He and H_2 have only two electrons, double exchange can only occur by double capture followed by radiative stabilization, sometimes called true double capture or stabilized double capture. Present results imply that double exchange for highly charged ions in CO_2 and H_2O proceeds predominately through triple capture followed by single Auger decay. Investigations by Sakaue *et al.* [31] have shown that this process is indeed the dominant mechanism for HCI's.

B. X-ray observations

A selection of x-ray spectra obtained from collisions of O^{7+}, O^{8+}, Ne^{9+}, and Ne^{10+} with He, H_2, H_2O, and CO_2, uncorrected for the transmission of the Be window, is shown in Figs. 4 and 5. Peaks in the spectra correspond to Ly transitions in H-like and He-like ions produced from single capture initially into $n=4$, 5, or 6. Contributions also arise from autoionization and radiative stabilization following multiple capture.

Gaussian profiles centered on the known transition energies have been fitted to the data. This fitting procedure gave an estimated full width at half maximum (FWHM) of 102 ± 2 eV, indicating that the Ge detector has a considerable resolution advantage over solid state detectors such as Si-Li (FWHM 170 eV) used in previous experiments [23,29].

Anisotropy in the photon emission can occur due to alignment of the collision system following preferential population of the substates of p levels. The intensity of the radiation $I(\theta)$ depends on the emission angle θ relative to the alignment axis (the ion beam direction), and is given by

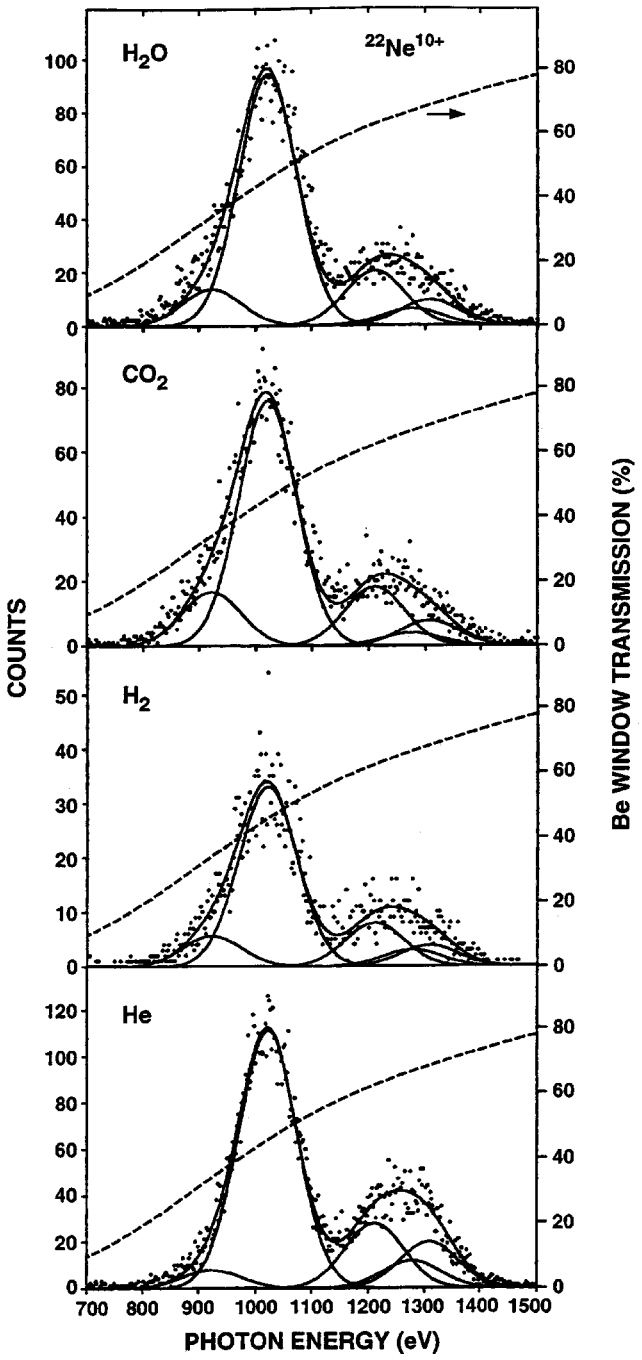

FIG. 4. X-ray spectra from collisions of Ne^{10+} in He, H_2, CO_2, and H_2O, uncorrected for transmission of the Be window on the Ge x-ray detector (given as a dashed line). The underlying curves are the Ly transitions $np \rightarrow 1s$.

$$I(\theta) = \frac{I_0(1 - P\cos^2\theta)}{1 - P/3}, \tag{6}$$

where P is the polarization and I_0 is the intensity at an angle of 54.7°. Previous work on $Ne^{9+} + H_2$ at a higher collision velocity [53] indicates that the polarization of the $2p$-$1s$ transitions is very small, as the transitions arise through many cascade paths. Higher transitions were observed to have $P = 0.6$. Given the lower collision velocities here, it is expected that alignment introduces an error of less than 15% for these transitions.

The relative contribution from each transition was determined from the area of the peaks fitted to the spectrum, divided by the transmission of the Be window. By normalizing the total spectrum to the charge-exchange results, emission cross sections were calculated. Results of the relative line-emission contributions for the collision systems studied are shown in Tables III and IV.

C. O^{8+} and Ne^{10+}

The x-ray spectra from collisions of fully stripped ions consists of contributions from both single and double capture. Cascading follows single capture, and only Ly transitions from p orbitals are energetic enough to be detected. A proportion of these cascades results in the population of the $2s$ metastable level that decays outside the detector viewing area. By assuming an initial distribution of nl states, the branching ratios determine the proportion decaying to the $2s$ state. If a statistical population of l states is assumed this fraction is less than 3.5% for $n \geqslant 4$, while for an even population it is less than 5%.

Double capture can be followed by radiative stabilization leading to He-like Lyman transitions, or by autoionization which preferentially populates $2p$ levels in the H-like ion [29], enhancing the Ly α ($2p \rightarrow 1s$) peak. It can be seen from Figs. 4 and 5 that the Ly α feature dominates the spectrum. Its intensity increases for higher charge states and lower ionization potentials of the target, with increasing value of the initial n state.

With the scheme of Vernhet *et al.* [23] it is possible to obtain information about the *average* angular momentum $\langle l \rangle$ of the initial capture state. Using a number of different theoretical predictions of the initial distribution of l states (including a statistical population), they showed that the relative contributions from the Lyman lines depended only on $\langle l \rangle$. From this analysis the ratio of the Ly α and Ly β lines can be used to obtain a value for $\langle l \rangle$, and these are given in Table III. It should be noted that this ratio might be contaminated with contributions from autoionizing double capture which tends to enhance the Ly α peak. Therefore the values of $\langle l \rangle$ should be regarded as upper limits.

The results show that the experimental values of $\langle l \rangle$ are consistently lower than that predicted by a statistical population. This is not surprising as (classically) the captured electron would not have enough angular momentum at a collision velocity of 0.35 a.u. (3 keV/amu) to be captured into $l = n - 1$. The values of $\langle l \rangle$ in Table III agree quite well with predictions of the overbarrier model, including a centrifugal barrier term [21].

For Ne^{10+} in all the targets there is a sizable double-exchange contribution from the $1s2p \rightarrow 1s^2$ transition in Ne^{8+} (915, 922 eV), seen as a low-energy shoulder in Fig. 4. Double capture in $Ne^{10+} + He$ has been investigated by several authors [30,33,34] who agree on the ratio of single to double capture (20%), but give different estimates of the stabilization ratio (30–50 %). A stabilization ratio of 40%

TABLE III. Cross sections (and errors) for x-ray emissions resulting from single or double capture by O^{8+} and Ne^{10+} projectiles. The ratio of Ly β to Ly α emission is shown and used to determine the average value of the initial angular momentum state of the captured electron $\langle l \rangle_{expt}$. This is compared to that determined from a statistical population of principal quantum number n, $\langle l \rangle_{stat}(n)$.

Projectile and transition	Transition energy (eV)	He	H_2	CO_2	H_2O
O^{7+}					
$2p\ ^2P_{3/2,1/2}-1s\ ^2S_{1/2}$ (Ly α)	570	1.8 (65%)	3.6 (69%)	4.6 (72%)	4.7 (75%)
$3p\ ^2P_{3/2,1/2}-1s\ ^2S_{1/2}$ (Ly β)	574	0.38 (13%)	0.91 (17%)	0.98 (15%)	0.95 (15%)
$4p\ ^2P_{3/2,1/2}-1s\ ^2S_{1/2}$ (Ly γ)	666	0.59 (21%)	0.37 (7%)	0.20 (3%)	0.15 (2%)
$5p\ ^2P_{3/2,1/2}-1s\ ^2S_{1/2}$ (Ly δ)	698	0.02 (1%)	0.39 (7%)	0.45 (7%)	0.42 (7%)
O^{6+}					
$1s2p\ ^3P_1,\ ^1P_1-1s^2\ ^1S_0$	570, 574	$\approx$0	$\approx$0	2.9%	1.1%
(Ly β)/(Ly α)		0.21	0.25	0.21	0.20
$\langle l \rangle_{expt}$		1.7	1.6	1.8	2.0
$\langle l \rangle_{stat}(n)$		2.13 (4)	2.80 (5)	2.80 (5)	2.80 (5)
Ne^{9+}					
$2p\ ^2P_{3/2,1/2}-1s\ ^2S_{1/2}$	1022	68%	65%	64%	68%
$3p\ ^2P_{3/2,1/2}-1s\ ^2S_{1/2}$	1211	13%	11%	11%	11%
$4p\ ^2P_{3/2,1/2}-1s\ ^2S_{1/2}$	1277	5%	4%	2%	3%
$5p,6p\ ^2P_{3/2,1/2}-1s\ ^2S_{1/2}$	1308, 1152	8%	5%	4%	5%
Ne^{8+}					
$1s2p\ ^3P_1,\ ^1P_1-1s^2\ ^1S_0$	915, 922	6.4%	15%	19%	13%
(Ly β)/(Ly α)		0.19	0.17	0.17	0.16
$\langle l \rangle_{expt}$		2.1	2.4	2.4	2.6
$\langle l \rangle_{stat}(n)$		2.80 (5)	3.47 (6)	3.47 (6)	4.14 (7)

gives a contribution of 8% from Ne^{8+} transitions, in close agreement with the present value of 6.4%. This contribution is larger for the multielectron targets CO_2 and H_2O, but for O^{8+} in all targets the contribution from O^{6+} transitions is very small (<3%). By contrast, a spectrum obtained by Vernhet *et al.* [23] for Al^{13+}+He showed a 40% contribution from Al^{11+} transitions. A systematic study by Martin *et al.* [33] for fully stripped ions showed that the stabilization ratio is high when symmetric doubly excited states are populated, and is only weakly dependent on the charge state.

D. O^{7+} and Ne^{9+}

For H-like projectiles, single capture results in the population of singlet or triplet He-like configurations. It has been suggested previously that the population of triplet and singlet

TABLE IV. Emission cross sections (and errors) for O^{7+} and Ne^{9+} projectiles on He, H_2, CO_2, and H_2O.

Projectile	Transition energy eV	He	H_2	CO_2	H_2O
O^{6+}					
$1s2p\ ^3P_1-1s^2\ ^1S_0$	570	0.29 (39%)	0.73 (39%)	1.11 (39%)	0.86 (39%)
$1s2p\ ^1P_1-1s^2\ ^1S_0$	574	0.19 (26%)	0.45 (24%)	0.94 (34%)	0.68 (31%)
$1s3p\ ^1P_1-1s^2\ ^1S_0$	666	0.15 (21%)	0.30 (17%)	0.39 (14%)	0.30 (14%)
$1s4p\ ^1P_1-1s^2\ ^1S_0$	698	0.10 (14%)	0.36 (20%)	0.33 (12%)	0.35 (16%)
Ne^{9+}					
$1s2p\ ^3P_1-1s^2\ ^1S_0$	915	0.44 (43%)	0.75 (43%)	1.3 (43%)	1.5 (43%)
$1s2p\ ^1P_1-1s^2\ ^1S_0$	922	0.38 (36%)	0.72 (40%)	1.5 (49%)	1.6 (46%)
$1s3p\ ^1P_1-1s^2\ ^1S_0$	1073	0.11 (10%)	0.18 (10%)	0.12 (4%)	0.20 (5%)
$1s4p\ ^1P_1-1s^2\ ^1S_0$	1127	0.08 (8%)	0.03 (2%)	0.07 (2%)	0.14 (4%)
$1s5p\ ^1P_1-1s^2\ ^1S_0$	1152	0.03 (3%)	0.09 (5%)	0.06 (2%)	0.07 (2%)

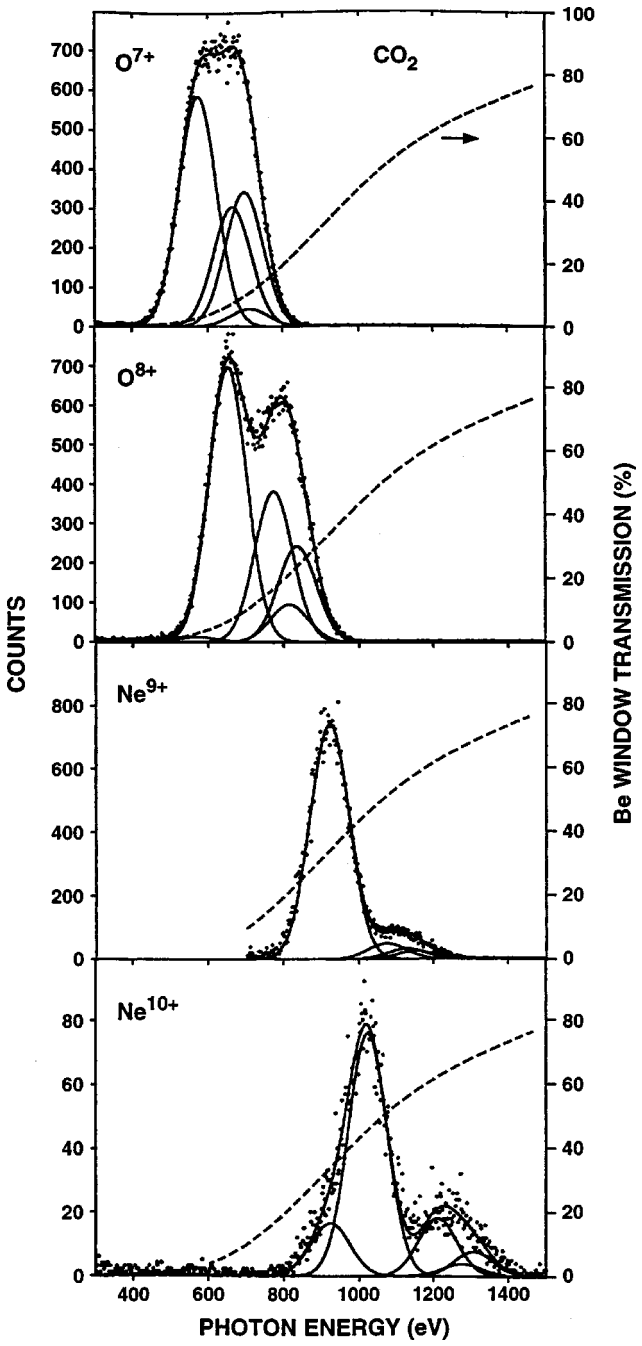

FIG. 5. X-ray spectra from collisions of O^{7+}, O^{8+}, Ne^{9+}, and Ne^{10+} in CO_2, uncorrected for transmission of the Be window on the Ge x-ray detector (given as a dashed line). The underlying curves are the Ly transitions $np \rightarrow 1s$.

levels be given by a statistical 3:1 ratio [7,24,25,35]. However, recent work has demonstrated that this ratio depends upon the collision velocity [54]. X rays are only emitted from singlet transitions to the ground state $1s^2\ ^1S$ with the exception of an intercombination transition $1s2p\ ^3P_1 \rightarrow 1s^2\ ^1S_0$ which has a short lifetime (O^{6+} 1.6 ns, branching ratio 87%; Ne^{8+} 0.18 ns, 98%).

The x-ray detector is unable to resolve the $^3P_1$ and $^1P_1$ transitions. Estimates of the relative contributions are presented in Table I, assuming that capture is three times more likely into triplet states. In previous work on He-like transitions [23,25] it was assumed that one-third of the capture into triplet levels cascades to the $2p\ ^3P_1$ state, with none to the $2s\ ^3S_1$ level. The present analysis of the branching ratios indicates roughly the same population of the $1s2s\ ^3S_1$ and $1s2p\ ^3P_1$ states (about 25%). When this is coupled with the branching ratio of the $1s2p\ ^3P_1 \rightarrow 1s^2\ ^1S_0$ transition, it is found that the intercombination transition contributes 39% to the total spectrum from O^{7+} projectiles, and 43% from Ne^{9+}. The relative intensities of transitions in $Ne^{9+}+H_2$ collisions are in very good agreement with previous work [23,53].

III. CONCLUSIONS

Accurate single and double charge-exchange cross sections have been measured for high charge states of C, N, O, and Ne in He, H_2, CO_2, and H_2O targets for collision energies of $7q$ keV. Results are in good agreement with previous results for He and H_2. It is noted that there is a dearth of results, both experimental and theoretical, for collisions in molecular targets such as H_2O, CO_2, and CO. Data on these species are needed to investigate the cometary x-ray emission phenomenon, and will have direct application to high-resolution spectra of comets expected from the two new orbiting x-ray telescopes, Chandra and Newton. Significant contribution from double exchange in many-electron targets, usually ignored in solar wind-comet models, has been highlighted.

X-ray spectra have been measured for these collision systems, and line-emission cross sections obtained. Analysis of the spectra has shown that the initial population of l states within a given n level is not weighted towards higher angular-momentum states as predicted by statistical population. The collision velocities attained (<0.35 a.u.) are insufficient to give the captured electron the required angular momentum, but the average value $\langle l \rangle$ is in agreement with the classical picture [21].

X-ray transitions from stabilized double capture have also been observed for Ne^{10+} projectiles, and the relative contributions are in good agreement with previous investigations of double-capture mechanisms. It is noted that for bare projectiles this contribution is strongly dependent on the availability of asymmetric doubly excited states, populated by autotransfer to Rydberg states and transfer excitation, which have a higher probability of radiative stabilization.

ACKNOWLEDGMENTS

This work was carried out at the Jet Propulsion Laboratory/Caltech, and was funded by the JPL Director's Discretionary Fund and NASA. J.B.G. acknowledges the support of the National Research Council through the Associateships Program and the Queen's University Belfast Research Fund. I.D.W. acknowledges support of both EPSRC and the QUB Research Fund.

[1] C. M. Lisse, K. Dennerl, J. Englhauser, M. Harden, F. E. Marshall, M. J. Mumma, R. Petre, J. P. Pye, M. J. Ricketts, J. Schmitt, J. Trumper, and R. G. West, Science **274**, 205 (1996).
[2] C. M. Lisse, D. Christian, K. Dennerl, J. Englhauser, J. Trumper, M. Desch, F. E. Marshall, R. Petre, and S. Snowden, Icarus **141**, 316 (1999).
[3] K. Dennerl, J. Englhauser, and J. Trumper, Science **277**, 1625 (1997).
[4] T. E. Cravens, Geophys. Res. Lett. **24**, 105 (1997).
[5] R. M. Haberli, T. I. Gombosi, D. L. De Zeeuw, M. R. Combi, and K. G. Powell, Science **276**, 939 (1997).
[6] R. Wegmann, H. U. Schmidt, C. M. Lisse, K. Dennerl, and J. Englhauser, Planet. Space Sci. **46**, 603 (1998).
[7] V. Kharchenko and A. Dalgarno, J. Geophys. Res. **105**, 18 351 (2000).
[8] M. Neugebauer, T. E. Cravens, C. M. Lisse, F. M. Ipavich, D. Christian, R. von Steiger, P. Bochsler, P. D. Shah, and T. P. Armstrong, J. Geophys. Res. **105**, 20 949 (2000).
[9] V. A. Krasnopolsky, M. J. Mumma, and M. J. Abbott, Icarus **146**, 152 (2000).
[10] C. Lisse, D. J. Christian, K. Dennerl, K. J. Meech, R. Petre, H. A. Weaver, and S. J. Wolk, Science (to be published).
[11] T. E. Cravens, Astrophys. J. Lett. **532**, L153 (2000).
[12] W. Liu and D. R. Schultz, Astrophys. J. **526**, 538 (1999).
[13] P. M. Stier and C. F. Barnett, Phys. Rev. **103**, 896 (1956).
[14] R. K. Janev, R. A. Phaneuf, and H. T. Hunter, At. Data Nucl. Data Tables **40**, 249 (1988).
[15] W. K. Wu, B. A. Huber, and K. Wiesemann, At. Data Nucl. Data Tables **40**, 58 (1988).
[16] M. Gargaud and R. McCarroll, J. Phys. B **18**, 463 (1985).
[17] L. F. Errea, J. D. Glorfinkiel, A. Macias, L. Mendez, and A. Riera, Phys. Scr. **T80B**, 185 (1999).
[18] A. Kumar and B. C. Saha, Phys. Rev. A **59**, 1273 (1999).
[19] H. Ryufuku, K. Sasaki, and T. Watanabe, Phys. Rev. A **21**, 745 (1980).
[20] A. Niehaus, J. Phys. B **19**, 2925 (1986).
[21] J. Burgdörfer, R. Morgenstern, and A. Niehaus, J. Phys. B **19**, L507 (1986).
[22] D. Dijkkamp, Yu. S. Gordeev, A. Brazuk, A. G. Drentje, and F. J. de Heer, J. Phys. B **18**, 737 (1985).
[23] D. Vernhet, A. Chetioui, J. P. Rozet, C. Stephan, K. Wohrer, A. Touati, M. F. Olitis, P. Bouisset, D. Hitz, and S. Dousson, J. Phys. B **21**, 3949 (1988).
[24] R. K. Janev and H. Winter, Phys. Rep. **117**, 265 (1985).
[25] M. G. Suraud, R. Hoekstra, F. J. de Heer, J. J. Bonnet, and R. Morgenstern, J. Phys. B **24**, 2543 (1991).
[26] V. A. Abramov, F. F. Baryshnikov, and V. A. Lisitsa, Pis'ma Zh. Eksp. Teor. Fiz. **27**, 494 (1978) [JETP Lett. **27**, 464 (1978)].
[27] R. Hoekstra, F. J. de Heer, and R. Morgenstern, J. Phys. B **24**, 4025 (1991).
[28] J.-Y. Chesnel, B. Sulik, H. Merabet, C. Bedouet, F. Fremont, X. Husson, M. Grether, A. Spieler, and N. Stolterfoht, Phys. Rev. A **57**, 3546 (1998).
[29] A. Chetioui, F. Martin, M. F. Politis, J. P. Rozet, A. Touati, L. Blumenfeld, D. Vernhet, K. Wohrer, C. Stephan, M. Barat, M. N. Gaboriaud, H. Laurent, and P. Roncin, J. Phys. B **23**, 3659 (1990).
[30] X. Fletchard, S. Duponchel, L. Adoui, A. Cassimi, P. Roncin, and D. Hennecart, J. Phys. B **30**, 3697 (1997).
[31] H. A. Sakaue *et al.*, Phys. Scr. **T73**, 182 (1997).
[32] S. Martin, J. Bernhard, L. Chen, A. Denis, and J. Desesquelles, Phys. Rev. A **52**, 1218 (1995).
[33] S. Martin, J. Bernhard, L. Chen, A. Denis, and J. Desesquelles, Phys. Scr. **T73**, 149 (1997).
[34] J.-Y. Chesnel, F. Fremont, B. Sulik, C. Ruiz-Mendez, H. Merabet, C. Bedouet, X. Husson, M. Grether, and N. Stolterfoht, Nucl. Instrum. Methods Phys. Res. B **154**, 142 (1999).
[35] M. Barat and P. Roncin, J. Phys. B **25**, 2205 (1992).
[36] J. B. Greenwood, A. Chutjian, and S. J. Smith, Astrophys. J. **529**, 605 (2000).
[37] J. B. Greenwood, I. D. Williams, S. J. Smith, and A. Chutjian, Astrophys. J. Lett. **533**, L175 (2000).
[38] A. Chutjian, J. B. Greenwood, and S. J. Smith, in *Atomic Process in Plasmas*, edited by E. Oks and M. S. Pindzola, AIP Conf. Proc. No. 443 (AIP, Woodburg, NY, 1998), p. 134.
[39] M. Knudsen, Ann. Phys. (Leipzig) **64**, 205 (1910).
[40] H. J. Blaauw, R. W. Wagenaar, D. H. Barends, and F. J. de Heer, J. Phys. B **13**, 359 (1980).
[41] J. P. Bromberg, J. Vac. Sci. Technol. **6**, 801 (1969).
[42] B. P. Mathur, J. E. Field, and S. O. Colgate, Phys. Rev. A **11**, 830 (1975).
[43] A. A. Smith, G. E. Derbyshire, R. C. Farrow, A. Sery, T. W. Raudorf, and M. Martini, Rev. Sci. Instrum. **66**, 2333 (1995).
[44] A. Itoh, N. Imanishi, F. Fukuzawa, N. Hamamoto, S. Hanawa, T. Tanaka, T. Ohdaira, M. Satio, Y. Haruyama, and T. Shirai, J. Phys. Soc. Jpn. **64**, 3255 (1995).
[45] D. H. Crandall, M. J. Mallory, and D. C. Kocher, Phys. Rev. A **15**, 61 (1977).
[46] R. Hoekstra, F. J. deHeer, and H. Winter, Nucl. Instrum. Methods Phys. Res. B **23**, 104 (1987).
[47] M. N. Panov, A. A. Basalaev and K. O. Lozhkin, Phys. Scr. **T3**, 124 (1983).
[48] V. V. Afrosimov, A. A. Basalaev, E. D. D. Donets, K. O. Lozhkin, and M. N. Panov, Pis'ma Zh. Eksp. Teor. Fiz. **34**, 179 (1981) [JETP Lett. **34**, 171 (1981)].
[49] R. A. Phaneuf, I. Alvarez, F. W. Meyer, and D. H. Crandall, Phys. Rev. A **26**, 1892 (1982).
[50] B. G. Lindsay, D. R. Sieglaff, K. A. Smith, and R. F. Stebbings, Phys. Rev. A **55**, 3945 (1997).
[51] A. Cassimi, S. Duponchel, A. Fletchard, P. Jardin, D. Hennecart, and R. E. Olson, Phys. Rev. Lett. **76**, 3679 (1996).
[52] M. Kimura, T. Iwai, Y. Kaneko, N. Kobayashi, A. Matsumoto, S. Ohtani, K. Okuno, S. Takagi, H. Tawara, and S. Tsurubuchi, J. Phys. Soc. Jpn. **53**, 2224 (1984).
[53] D. Vernhet, A. Chetioui, K. Wohrer, J. P. Rozet, P. Piqumal, D. Hitz, S. Dousson, A. Salin, and C. Stephan, Phys. Rev. A **32**, 1256 (1985).
[54] F. W. Bliek, G. R. Woestenenk, R. Hoekstra, and R. Morgenstern, Phys. Rev. A **57**, 221 (1998).